Synthesis, Characterization and Electrochemistry of Lithium Battery Electrodes: $xLi_2MnO_3\cdot(1-x)LiMn_{0.333}Ni_{0.333}Co_{0.333}O_2$ $(0 \leq x \leq 0.7)$

Christopher S. Johnson,* Naichao Li,† Christina Lefief, John T. Vaughey, and Michael M. Thackeray

Electrochemical Energy Storage Department, Chemical Sciences and Engineering Division, Argonne National Laboratory, Argonne, Illinois 60439

Received May 6, 2008. Revised Manuscript Received July 18, 2008

Lithium- and manganese-rich layered electrode materials, represented by the general formula $xLi_2MnO_3\cdot(1-x)LiMO_2$ in which M is Mn, Ni, and Co, are of interest for both high-power and high-capacity lithium ion cells. In this paper, the synthesis, structural and electrochemical characterization of $xLi_2MnO_3\cdot(1-x)LiMn_{0.333}Ni_{0.333}Co_{0.333}O_2$ electrodes over a wide compositional range ($0 \leq x \leq 0.7$) is explored. Changes that occur to the compositional, structural, and electrochemical properties of the electrodes as a function of x and the importance of using a relatively high manganese content and a high charging potential (>4.4 V) to generate high capacity (>200 mAh/g) electrodes are highlighted. Particular attention is given to the electrode composition $0.3Li_2MnO_3\cdot0.7LiMn_{0.333}Ni_{0.333}Co_{0.333}O_2$ ($x = 0.3$) which, if completely delithiated during charge, yields $Mn_{0.533}Ni_{0.233}Co_{0.233}O_2$, in which the manganese ions are tetravalent and, when fully discharged, $LiMn_{0.533}Ni_{0.233}Co_{0.233}O_2$, in which the average manganese oxidation state (3.44) is marginally below that expected for a potentially damaging Jahn−Teller distortion (3.5). Acid treatment of $0.3Li_2MnO_3\cdot0.7LiMn_{0.333}Ni_{0.333}Co_{0.333}O_2$ composite electrode structures with 0.1 M HNO_3 chemically activates the Li_2MnO_3 component and essentially eliminates the first cycle capacity loss but damages electrochemical behavior, consistent with earlier reports for Li_2MnO_3-stabilized electrodes. Differences between electrochemical and chemical activation of the Li_2MnO_3 component are discussed. Electrochemical charge/discharge profiles and cyclic voltammogram data suggest that small spinel-like regions, generated in cycled manganese-rich electrodes, serve to stabilize the electrodes, particularly at low lithium loadings (high potentials). The study emphasizes that, for high values of x, a relatively small $LiMO_2$ concentration stabilizes a layered Li_2MnO_3 electrode to reversible lithium insertion and extraction when charged to a high potential.

Introduction

Structurally integrated $xLi_2M'O_3\cdot(1-x)LiMO_2$ electrode materials, in which M′ is selected typically from Mn and Ti; and M from Mn, Ni, and Co, are promising cathodes (positive electrodes) for lithium ion batteries.[1] The structural compatibility between the layered $Li_2M'O_3$ and $LiMO_2$ components allows integration to occur at the nanoscopic level and the possibility of tailoring the composition of the electrode to achieve optimum performance.[2] Such integrated electrode structures offer superior cost and safety features over state-of-the-art $LiCoO_2$ electrodes that typically power today's commercial lithium ion batteries in laptop computers and wireless communication devices. The $xLi_2MnO_3\cdot(1-x)LiMO_2$ electrodes cycle with excellent stability and can be charged and discharged at relatively high rates, particularly for low values of x ($x \sim 0.1$), making them excellent candidates to replace $LiCoO_2$.[1,2] When higher values of x are used and if the Li_2MnO_3 ($Li_2O\cdot MnO_2$) component is electrochemically activated above 4.4 V to remove Li_2O from the electrode structure on charge, then the electrodes can deliver a capacity above 200 mAh/g between 4.6 and 3.0 V. Such a high capacity should allow the fabrication of lithium ion cells with sufficiently high energy to power "plug-in" hybrid electric vehicles if adequate rate and cycle life can also be provided by the electrode.[3]

Over the past several years, there have been concerted efforts to design Mn-based layered $LiMO_2$ compounds in attempts to find a less expensive and safer cathode material than $LiCoO_2$. Although it is possible to synthesize a layered MnO_2 compound by leaching Li_2O from Li_2MnO_3 with acid[4,5] and a layered $LiMnO_2$ compound by ion exchange from $NaMnO_2$,[6,7] these materials have not provided the structural or electrochemical stability to make them viable

* Corresponding author. Phone: (630)-252-4787. Fax: (630)-252-4176. E-mail: cjohnson@anl.gov.

† Current Address: 3M Corporation, St. Paul, MN 55144.

(1) Thackeray, M. M.; Kang, S.-H.; Johnson, C. S.; Vaughey, J. T.; Benedek, R.; Hackney, S. A. *J. Mater. Chem.* **2007**, *17*, 3112.

(2) Thackeray, M. M.; Kang, S.-H.; Johnson, C. S.; Vaughey, J. T.; Hackney, S. A. *Electrochem. Commun.* **2006**, *8*, 1531.

(3) Thackeray, M. M.; Johnson, C. S.; Vaughey, J. T.; Li, N.; Hackney, S. A. *J. Mater. Chem.* **2005**, *15*, 2257.

(4) Rossouw, M. H.; Thackeray, M. M. *Mater. Res. Bull.* **1991**, *26*, 463.

(5) Johnson, C. S.; Korte, S. D.; Vaughey, J. T.; Thackeray, M. M.; Bofinger, T. E.; Shao-Horn, Y.; Hackney, S. A. *J. Power Sources* **1999**, *81*, 491.

(6) Armstrong, A. R.; Bruce, P. G. *Nature* **1996**, *381*, 499.

(7) Capitaine, F.; Gravereau, P.; Delmas, C. *Solid State Ionics* **1996**, *89*, 197.

10.1021/cm801245r CCC: $40.75
Published on Web 09/20/2008

candidates to replace $LiCoO_2$. Greater stability has been achieved by combining Mn with either Ni or Ni and Co in layered $LiMO_2$ frameworks; in this respect, the best known and most widely exploited materials are $LiMn_{0.5}Ni_{0.5}O_2$[8−10] and $LiMn_{0.333}Ni_{0.333}Co_{0.333}O_2$ (alternatively, $Li(Mn_{1/3}Ni_{1/3}Co_{1/3})O_2$ or $Li(MnNiCo)_{1/3}O_2$).[11−16] Recent developments have shown that higher capacity electrodes and an improved rate capability can be achieved if excess lithium is added to $LiMn_{0.5}Ni_{0.5}O_2$ and $LiMn_{0.333}Ni_{0.333}Co_{0.333}O_2$ electrodes.[17−20] To maintain the rocksalt stoichiometry, in which the number of cations equals the number of anions, these lithium-rich electrodes are formulated $Li_{1+x}(Mn_{0.5}Ni_{0.5})_{1-x}O_2$ and $Li_{1+x}(Mn_{0.333}Ni_{0.333}Co_{0.333})_{1-x}O_2$, respectively.[2] Because nearest-neighbor Mn and Ni ions tend to adopt tetravalent and divalent oxidation states, respectively,[21,22] rather than two trivalent states, by combining the excess monovalent Li ions with the tetravalent Mn ions, it is possible to reformulate the composition of the electrodes in two-component notation, $xLi_2MnO_3\cdot(1-x)LiMO_2$ (M = Mn, Ni, Co). For example, the compound $Li_{1.1}Mn_{0.333}Ni_{0.333}Co_{0.333}O_{2.1}$ (rocksalt stoichiometry) that contains 10% excess lithium can be rewritten either as $0.10Li_2MnO_3\cdot0.90LiMn_{0.26}Ni_{0.37}Co_{0.37}O_2$ or, in conventional layered notation, as $Li[Li_{0.0475}Mn_{0.3175}Ni_{0.3175}Co_{0.3175}]O_2$ or $Li_{1.0475}[Mn_{0.333}Ni_{0.333}Co_{0.333}]_{0.9525}O_2$. This electrode material, which has a highly complex structure, shows excellent electrochemical properties, particularly when preconditioned with mildly acidic fluorinated solutions; it provides a stable discharge capacity of 170−175 mAh/g when cycled between 4.6 and 3.0 V in lithium ion cells.[1]

We have focused our earlier work on $xLi_2MnO_3\cdot(1-x)LiMO_2$ electrodes in which M is Mn and Ni, with compositions within the $xLi_2MnO_3\cdot(1-x)LiMn_{0.5}Ni_{0.5}O_2$ system.[23,24] In this paper, we report the synthesis and structural and electrochemical characterization of Li_2MnO_3-stabilized $LiMn_{0.333}Ni_{0.333}Co_{0.333}O_2$ electrodes over a wide compositional range ($0 \geq x \geq 0.7$). The work builds on our earlier communication on $xLi_2MnO_3\cdot(1-x)LiMn_{0.333}Ni_{0.333}Co_{0.333}O_2$ electrode materials that can deliver anomalously high capacities when they contain a high Li_2MnO_3 content ($x = 0.5$ and $x = 0.7$).[25] This article focuses on changes that occur to the structural and electrochemical properties of the electrodes as a function of x. The effects of chemical activation by acid treatment to remove Li_2O from the Li_2MnO_3 component on electrochemical behavior are compared to the effects of electrochemical activation.[26,27]

Experimental Section

Cathode materials $xLi_2MnO_3\cdot(1-x)LiMn_{0.333}Ni_{0.333}Co_{0.333}O_2$ ($0 \leq x \leq 0.7$) were prepared from lithium hydroxide hydrate ($LiOH\cdot H_2O$) and manganese−nickel−cobalt hydroxide precursors using the required amounts of Mn, Ni, Co, and Li for a given value of x. The transition metal hydroxide materials were prepared by coprecipitation of the required hydrated metal nitrate salts, $Mn(NO_3)_2\cdot4H_2O$, $Ni(NO_3)_2\cdot6H_2O$, and $Co(NO_3)_2\cdot6H_2O$, under basic conditions with lithium hydroxide hydrate ($LiOH\cdot H_2O$) in water at room temperature to 50 °C. The pH was adjusted to around 11 during the precipitation reaction by addition of ammonium hydroxide (NH_4OH) solution. Precipitates were isolated by vacuum filtration and washed multiple times with distilled deionized water. The precipitate was intimately mixed with $LiOH\cdot H_2O$ at the desired stoichiometry and then fired in air, first between 300−500 °C for 3−6 h and then again as a pellet between 800−1000 °C for 3−5 h. A 3 wt % excess of $LiOH\cdot H_2O$ was used as a precaution to offset any lithium evaporative losses. The products were cooled to room temperature in the box furnace. For comparison, a high-temperature sample of bulk Li_2MnO_3 was synthesized from lithium carbonate and manganese carbonate at 1000 °C in air. Acid treatment of powders ($x = 0$, 0.1, 0.2, and 0.3) was undertaken by reaction with 0.1 M HNO_3 (50 mL/g oxide) with constant stirring for either 5 or 24 h at room temperature. During this process, the pH of the solution was monitored (Corning pH meter, model 445). Products were filtered, washed, and oven-dried at 100 °C in air. Thereafter, the powders were reground and heated further at 480 °C for 5 h in air to remove residual surface and occluded water. Inductively coupled plasma atomic emission spectrometry (ICP-AES) analyses were conducted on the final products ($0 \leq x \leq 0.3$) and on the acid-leached sample ($x = 0.3$) using an Atomscan Advantage (Thermo Jarrell Ash) spectrometer to determine the relative amounts of Li, Mn, Ni, and Co in the samples.

X-ray diffraction (XRD) patterns of the electrode materials were collected on a Siemens D5000 powder diffractometer with Cu Kα radiation between 5 and 80° 2θ at a scan rate of 0.6° 2θ/min. Lattice parameters of the $xLi_2MnO_3\cdot(1-x)LiMn_{0.333}Ni_{0.333}Co_{0.333}O_2$ samples over the full range of x ($0 \leq x \leq 1.0$) were determined by Rietveld refinement of their XRD patterns using the software program GSAS.[28] The particle morphology of the $xLi_2MnO_3\cdot(1-x)LiMn_{0.333}Ni_{0.333}Co_{0.333}O_2$ powders and acid-leached products were examined by scanning electron microscopy (SEM) on a Hitachi S-4700-II instrument.

Electrode laminates were made by casting a slurry of 84% active oxide (by weight), 4% graphite (Timcal, SFG-6), 4% carbon black (Toka), and 8% PVDF binder (Kynar) in *N*-methyl-2-pyrrolidinone

(8) Ohzuku, T.; Makimura, Y. *Chem. Lett.* **2001**, 744.
(9) Johnson, C. S.; Kim, J.-S.; Kropf, A. J.; Kahaian, A. J.; Vaughey, J. T.; Fransson, L. M. L.; Edström, K.; Thackeray, M. M. *Chem. Mater.* **2003**, *15*, 2313.
(10) Bregér, J.; Kang, K.; Cabaña, J.; Ceder, G.; Grey, C. P. *J. Mater. Chem.* **2007**, *17*, 3167.
(11) Yabuuchi, N.; Ohzuku, T. *J. Power Sources* **2003**, *119*, 171.
(12) Yabuuchi, N.; Koyama, Y.; Nakayama, N.; Ohzuku, T. *J. Electrochem. Soc.* **2005**, *152*.
(13) Choi, J.; Manthiram, A. *J. Electrochem. Soc.* **2005**, *152*, A1714.
(14) Cho, T. H.; Park, S. M.; Yoshio, M.; Hirai, T.; Hideshima, Y. *J. Power Sources* **2005**, *142*, 306.
(15) Lee, M. H.; Kang, Y.; Myung, S. T.; Sun, Y. K. *Electrochim. Acta* **2004**, *50*, 939.
(16) Wang, Z. X.; Sun, Y. C.; Chen, L. Q.; Huang, X. J. *J. Electrochem. Soc.* **2004**, *151*, A914.
(17) Kang, S.-H.; Park, S.-H.; Johnson, C. S.; Amine, K. *J. Electrochem. Soc.* **2007**, *154*, A268.
(18) Park, S.-H.; Kang, S.-H.; Belharouak, I.; Sun, Y. K.; Amine, K. *J. Power Sources* **2008**, *177*, 177.
(19) Kim, J.-M.; Kumagai, N.; Chung, H.-T. *Electrochem. Solid State Lett.* **2006**, *9*, A494.
(20) Todorov, Y. M.; Numata, K. *Electrochim. Acta* **2004**, *50*, 495.
(21) Yoon, W. S.; Grey, C. P.; Balasubramanian, M.; Yang, X. Q.; Fischer, D. A.; McBreen, J. *Electrochem. Solid State Lett.* **2004**, *7*, A53.
(22) Deb, A.; Cairns, E. J. *Fluid Phase Equilib.* **2006**, *241*, 4.
(23) Kim, J.-S.; Johnson, C. S.; Vaughey, J. T.; Thackeray, M. M.; Hackney, S. A.; Yoon, W.-S.; Grey, C. P. *Chem. Mater.* **2004**, *16*, 1996.
(24) Kim, J.-S.; Johnson, C. S.; Vaughey, J. T.; Thackeray, M. M. *J. Power Sources* **2006**, *153*, 258.
(25) Johnson, C. S.; Li, N.; Lefief, C.; Thackeray, M. M. *Electrochem. Commun.* **2007**, *9*, 787.
(26) Kang, S.-H.; Johnson, C. S.; Vaughey, J. T.; Amine, K.; Thackeray, M. M. *J. Electrochem. Soc.* **2006**, *153*, A1186.
(27) Johnson, C. S.; Kim, J.-S.; Lefief, C.; Li, N.; Vaughey, J. T.; Thackeray, M. M. *Electrochem. Commun.* **2004**, *6*, 1085.
(28) Larson, A. C.; Von Dreele, R. B. GSAS-General Structure Analysis System, Report No. LA-UR-86−748; Los Alamos National Laboratory; Los Alamos, NM, 1990.

Table 1. Composition of $xLi_2MnO_3\cdot(1-x)LiMn_{0.333}Ni_{0.333}Co_{0.333}O_2$ Electrode Materials

x	Mn/Ni/Co ratio in metal hydroxide precursor ($y \sim 2$)	Li/Mn/Ni/Co ratio expected (with 3 wt % Li evaporative loss)	Li/Mn/Ni/Co ratio experimental (AES-ICP)
0	$(Mn_{0.33}Ni_{0.33}Co_{0.33})(OH)_y$	1.00:0.33:0.33:0.33	1.13:0.33:0.33:0.32
0.1	$(Mn_{0.40}Ni_{0.30}Co_{0.30})(OH)_y$	1.10:0.40:0.30:0.30	1.21:0.40:0.30:0.29
0.2	$(Mn_{0.46}Ni_{0.27}Co_{0.27})(OH)_y$	1.20:0.46:0.27:0.27	1.30:0.46:0.27:0.26
0.3	$(Mn_{0.53}Ni_{0.23}Co_{0.23})(OH)_y$	1.30:0.53:0.23:0.23	1.38:0.53:0.23:0.23
0.3, 5-h acid-treated	$(Mn_{0.53}Ni_{0.23}Co_{0.23})(OH)_y$		1.14:0.53:0.23:0.23
0.3, 24-h acid-treated	$(Mn_{0.53}Ni_{0.23}Co_{0.23})(OH)_y$		1.10:0.53:0.23:0.23
0.5	$(Mn_{0.66}Ni_{0.17}Co_{0.17})(OH)_y$	1.50:0.66:0.17:0.17	
0.7	$(Mn_{0.80}Ni_{0.10}Co_{0.10})(OH)_y$	1.70:0.80:0.10:0.10	

(NMP) solvent onto an Al foil substrate. The slurry was cast using a doctor blade. The cast laminates were dried, first in air at 75 °C for 1−2 h, then in vacuum at 70 °C overnight. They were pinch-rolled to a fixed thickness of 40−70 μm. Lithium coin cells (Hohsen Corporation, size 2032) were constructed in an Ar-filled glovebox (Vacuum Atmospheres; <5 ppm O_2). The electrolyte was 1 M $LiPF_6$ in 1:1 EC/DEC (Merck). The counter electrode (anode) was lithium metal (FMC Corporation, Lithium Division). Cells were cycled galvanostatically at room temperature or 50 °C using a Maccor series 2000 battery tester at a constant current rate of either 0.05 or 0.1 mA/cm^2 with voltage window between 4.6 and 2.5 V, 4.6 and 2.0 V, or 4.3 and 2.0 V. Cyclic voltammograms of the electrode materials were recorded in lithium cells with a Solartron 1480 potentiostat at room temperature between 5.0 and 2.0 V at a sweep rate of 0.02 mV/s (20 μV/s).

Results and Discussion

Compositional Analysis and X-ray Diffraction. Table 1 lists the compositions of the six $xLi_2MnO_3\cdot(1-x)LiMn_{0.333}Ni_{0.333}Co_{0.333}O_2$ electrode materials synthesized for this study in terms of x and the corresponding Li/Mn/Ni/Co ratios in the transition metal hydroxide precursors from which the materials were made. Table 1 also provides the experimentally measured Li/Mn/Ni/Co mole ratio as determined by AES-ICP analysis for $x = 0.1$, $x = 0.2$ and 0.3, and two acid-treated samples derived from the sample with $x = 0.3$ (5-h and 24-h leach). The experimentally determined Mn/Ni/Co ratios are in excellent agreement with the target stoichiometries, whereas the experimentally determined lithium values were, on average, approximately 10% higher than anticipated but consistent, within experimental error, with the 3 wt % excess lithium that was used to offset the possible evaporative loss of lithium. The data shows that little of the excess lithium used was actually lost during synthesis. In the absence of any detectable lithium-containing byproduct in the XRD patterns, such as Li_2CO_3, we conclude that the surplus lithium was incorporated within the $xLi_2MnO_3\cdot(1-x)LiMn_{0.333}Ni_{0.333}Co_{0.333}O_2$ structures. Any surplus lithium would marginally increase the value of x and slightly change the Mn/Ni/Co ratio in the $LiMn_{0.333}Ni_{0.333}Co_{0.333}O_2$ component of the various electrode materials. However, because of the difficulty in determining the precise formula of the materials, we use the nominal compositions $x = 0$, 0.1, 0.2, 0.3, 0.5, 0.7, and 1.0 to describe the materials in this paper for simplicity and convenience.

The X-ray diffraction patterns of $xLi_2MnO_3\cdot(1-x)LiMn_{0.333}Ni_{0.333}Co_{0.333}O_2$ products prepared at 900 °C for $x = 0$, 0.1, 0.2, 0.3, 0.5, and 0.7 are shown in Figure 1(a−f), respectively. For the lattice parameter refinements of the $xLi_2MnO_3\cdot(1-x)LiMn_{0.333}Ni_{0.333}Co_{0.333}O_2$ structures, the symmetry of the crystal lattice was approximated to be trigonal ($R\bar{3}m$), which excludes the low-intensity reflections characteristic of the Li_2MnO_3-like regions in the XRD patterns, in particular, those at 21−25° 2θ; this procedure is commonly used in the refinements of these highly complex, structurally integrated materials.[1−3] The (020) reflection at ~21° 2θ, which is characteristic of the integrated monoclinic Li_2MnO_3-like component ($C2/m$) and due to the Li cation ordering in the metal layer, is highlighted by the arrow in Figure 1(b−f). This peak increases significantly with increasing x, as expected, for compositions along the $Li_2MnO_3-LiMn_{0.333}Ni_{0.333}Co_{0.333}O_2$ tieline of the $Li_2MnO_3-LiMn_{0.333}Ni_{0.333}Co_{0.333}O_2-MO_2$ phase diagram (Figure 2), in which the MO_2 composition of the charged electrode is a variable, $M = Mn_{1-2\delta}Ni_\delta Co_\delta$. The value of δ is dependent on the initial composition of the electrode (x), whereas the composition of the charged $xLi_2MnO_3\cdot(1-x)LiMn_{0.333}Ni_{0.333}Co_{0.333}O_2$ electrode depends on the extent to which lithia (Li_2O) is extracted from the electrode (i.e., along the $Li_2MnO_3-Mn_{1-2\delta}Ni_\delta Co_\delta$ tieline in Figure 2) at high potential (>4.4 V). The dashed line in Figure 2 tracks the initial extraction of lithium from the $LiMn_{0.333}Ni_{0.333}Co_{0.333}O_2$ component of a $0.3Li_2MnO_3\cdot0.7LiMn_{0.333}Ni_{0.333}Co_{0.333}O_2$ electrode, whereas the dotted line tracks the subsequent reversible discharge/charge reaction of the electrode that still contains a relatively small amount of unactivated, stabilizing Li_2MnO_3.[27]

Of particular interest to this study is the electrode composition $0.3Li_2MnO_3\cdot0.7LiMn_{0.333}Ni_{0.333}Co_{0.333}O_2$ ($x = 0.3$) which, if fully delithiated (activated), would yield $Mn_{0.533}Ni_{0.233}Co_{0.233}O_2$; in this instance, $\delta = 0.233$. When discharged back to the rock salt stoichiometry, the electrode composition becomes $LiMn_{0.533}Ni_{0.233}Co_{0.233}O_2$, in which the average manganese oxidation state of 3.44, assuming divalent nickel and trivalent cobalt, is marginally below that expected for a potentially damaging Jahn−Teller distortion (3.5). In practice, however, it is difficult to extract all the lithium electrochemically from the electrode structure. It might be expected, therefore, that of the $xLi_2MnO_3\cdot(1-x)LiMn_{0.333}Ni_{0.333}Co_{0.333}O_2$ electrodes selected for this investigation, the composition $x = 0.3$ might yield the most stable, high-capacity electrode, particularly if a residual amount of lithium remained in the structure after electrochemical activation that would drive the average manganese oxidation state toward 3.5 or above, as illustrated in Figure 2. This composition ($x = 0.3$) was, therefore, selected for many of our investigations, particularly the acid-treatment experiments (later section).

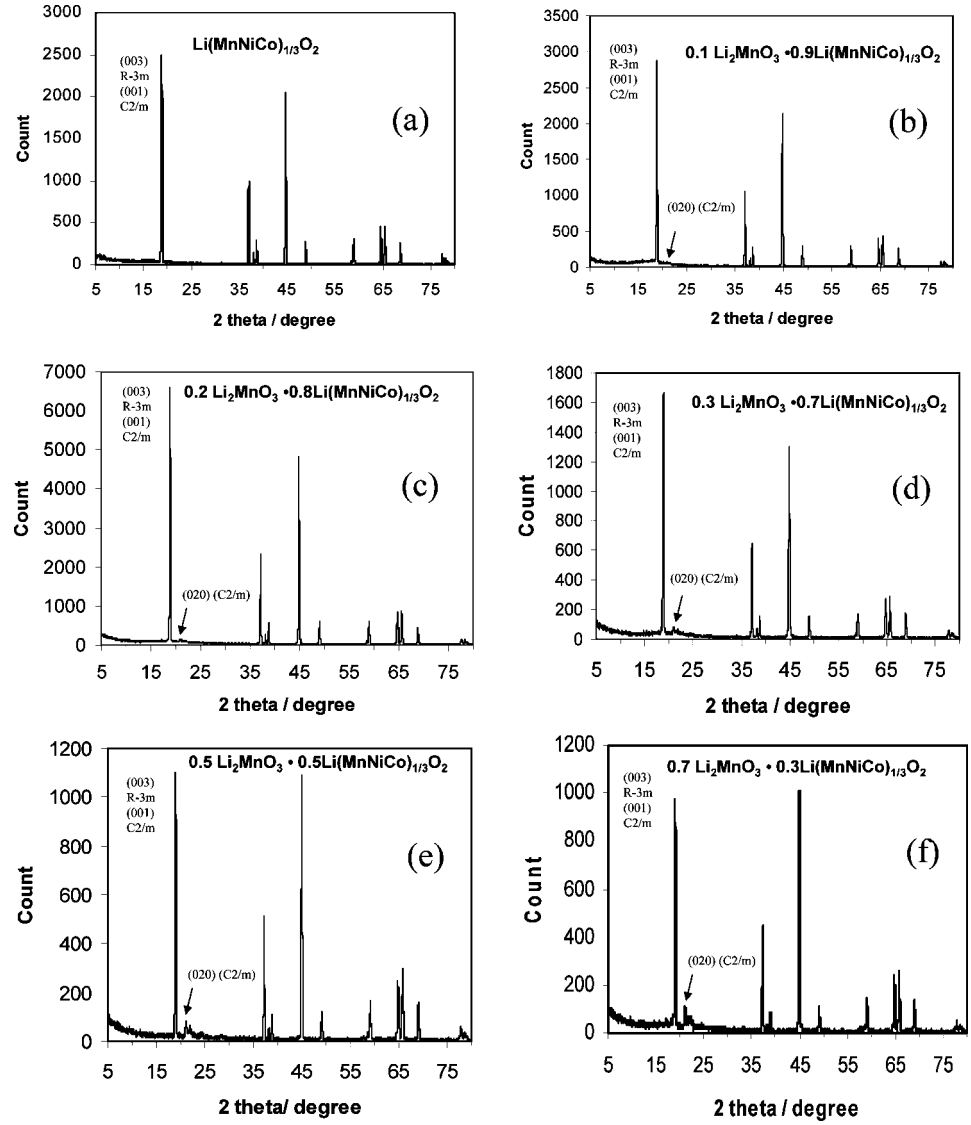

Figure 1. Powder X-ray diffraction patterns of $x\mathrm{Li_2MnO_3}\cdot(1-x)\mathrm{LiMn_{0.333}Ni_{0.333}Co_{0.333}O_2}$ materials for (a) $x = 0$, (b) $x = 0.1$, (c) $x = 0.2$, (d) $x = 0.3$, (e) $x = 0.5$, and (f) $x = 0.7$.

Despite the limitation placed on crystal symmetry, the lattice parameter refinements made it possible to observe the general trend of the *c*/*a* ratio in a pseudotrigonal unit cell as a function of *x*, thereby providing information about the effect of Li_2MnO_3 content on the interlayer spacing of the closely packed structures (Table 2). Table 2 includes the *c*/*a* ratio for the essentially cubic-close-packed Li_2MnO_3 structure when approximated to trigonal $R\bar{3}m$ symmetry. Table 2 also provides the formulas of the various $x\mathrm{Li_2MnO_3}\cdot(1-x)$-$\mathrm{LiMn_{0.333}Ni_{0.333}Co_{0.333}O_2}$ materials in standard $\mathrm{Li[M]O_2}$ notation (M = Li, Mn, Ni, Co) to highlight the increase in Li and Mn content relative to Co and Ni with increasing *x*. Various similar compositions which have been written instead with the $\mathrm{Li[M]O_2}$ notation have been widely reported in the literature.[29−36] Plots of the *c*/*a* ratio and manganese content vs composition, *x*, are shown in Figure 3a. Whereas the percent Mn tracks linearly with *x*, the *c*/*a* ratio plot is parabolic. The shape of the *c*/*a* ratio plot is attributed largely to differences in the relative rates of change in *c* and *a* (Table 2) and in particular to a shrinking *a* lattice parameter. The interlayer spacing, reflected by the *c* parameter, remains essentially constant for $0 \le x \le 3$ but thereafter increases slightly from 14.217 Å ($x = 0.3$) to 14.239 Å ($x = 0.7$) to 14.268 Å ($x = 1.0$) for the end-member Li_2MnO_3 fitted using a "pseudotrigonal" symmetry, $R\bar{3}m$. The decrease in the value

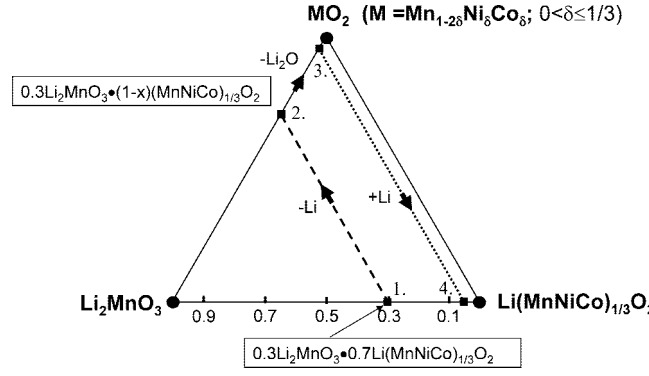

Figure 2. Compositional phase diagram of a $Li_2MnO_3-LiMn_{0.333}Ni_{0.333}$-$Co_{0.333}O_2-MO_2$ system in which the MO_2 apex is a variable, M = $Mn_{1-2\delta}Ni_\delta Co_\delta$.

(29) Lu, Z.; Beaulieu, L. Y.; Donaberger, R. A.; Thomas, C. L.; Dahn, J. R. *J. Electrochem. Soc.* **2002**, *149*, A778.

Table 2. Refined Lattice Parameters of xLi$_2$MnO$_3$·(1 − x)LiMn$_{0.333}$Ni$_{0.333}$Co$_{0.333}$O$_2$ Compounds According to Approximate $R\bar{3}m$ Symmetry

x	alternative Li[M]O$_2$ notation	a (Å)	c (Å)	c/a
0	Li[Mn$_{0.333}$Ni$_{0.333}$Co$_{0.333}$]O$_2$	2.8565(1)	14.217(1)	4.977
0.1	Li[Li$_{0.048}$Mn$_{0.381}$Ni$_{0.286}$Co$_{0.286}$]O$_2$	2.8539(1)	14.217(1)	4.982
0.2	Li[Li$_{0.091}$Mn$_{0.424}$Ni$_{0.242}$Co$_{0.242}$]O$_2$	2.8514(1)	14.220(1)	4.987
0.3	Li[Li$_{0.130}$Mn$_{0.464}$Ni$_{0.203}$Co$_{0.203}$]O$_2$	2.8493(1)	14.217(1)	4.990
0.5	Li[Li$_{0.200}$Mn$_{0.533}$Ni$_{0.133}$Co$_{0.133}$]O$_2$	2.8483(2)	14.228(2)	4.995
0.7	Li[Li$_{0.259}$Mn$_{0.593}$Ni$_{0.074}$Co$_{0.074}$]O$_2$	2.8490(1)	14.239(2)	4.998
1.0	Li[Li$_{0.333}$Mn$_{0.667}$]O$_2$	2.8439(2)	14.228(2)	5.003

of a is attributed to the increasing Mn^{4+} ion content because tetravalent manganese has a smaller ionic radius in octahedral coordination (0.54 Å) relative to high-spin Mn^{3+} (0.65 Å), low-spin Ni^{3+} (0.56 Å), Ni^{2+} (0.70 Å), high-spin Co^{3+} (0.61 Å), and low-spin Co^{2+} (0.65 Å),[37] all of which might be present at various levels in these highly complex integrated structures.[2] Our conclusion is consistent with the Mn(IV)−O bond lengths, calculated from the Rietveld refinement of the X-ray diffraction data for the end members of the composite series with a value of 1.9287 Å in LiMn$_{0.333}$Ni$_{0.333}$Co$_{0.333}$O$_2$ (Table 2) and 1.9229 Å in Li$_2$MnO$_3$ (Table 2).[38] The data in Figure 3a are also consistent with the notion that the Li$_2$MnO$_3$ and LiMn$_{0.333}$Ni$_{0.333}$Co$_{0.333}$O$_2$ components are in equilibrium with one other in these complicated structures.

With regard to the complex atomic arrangements in xLi$_2$MnO$_3$·(1 − x)LiMn$_{0.333}$Ni$_{0.333}$Co$_{0.333}$O$_2$ structures, it is worth commenting that for low values of x, typically less than 0.05, it is sometimes difficult to determine the Li$_2$MnO$_3$-like structural features by powder X-ray diffraction methods;[2] for low amounts of excess lithium, more powerful analytical methods specific to local metal environments, such as solid state NMR or Raman spectroscopy, can be used to identify these features. Considerable success has been achieved by Clare Grey's group in exploiting NMR techniques to unravel the local structure of these complex materials.[33,39] Jeong et al. have also recently demonstrated by Raman spectroscopy that it is possible to identify the symmetry characteristics of an Li$_2$MnO$_3$-type component in Li[Li$_{0.07}$Ni$_{0.1}$Co$_{0.6}$Mn$_{0.23}$]O$_2$ (0.17Li$_2$MnO$_3$·0.93LiMn$_{0.032}$Ni$_{0.138}$Co$_{0.83}$O$_2$) electrodes.[40] Using resonant diffraction methods at an X-ray synchrotron light source, Whitfield et al. recently differentiated the Mn atomic positions versus Ni/Co positions in the Li-rich compound Li$_{1.2}$Mn$_{0.4}$Ni$_{0.3}$Co$_{0.1}$O$_2$.[41] The refined structure (*C*2/*m* monoclinic symmetry) showed that the metal cations were not randomly distributed over the octahedral 4*g* and 2*b* sites in the transition-metal layers, the manganese and lithium ions preferring the 4*g* and 2*b* sites, respectively (as in Li$_2$MnO$_3$), while the cobalt and nickel ions showed a preference for the larger 2*b* site over the 4*g* site.

The increase in magnitude of the weak (020) ordering peak at ∼21° 2θ, which represents the Li$_2$MnO$_3$-like component with monoclinic symmetry (*C*2/*m*), relative to the strong, overlapping $(001)_{C2/m}$ and $(003)_{R3^-m}$ peaks at ∼18° 2θ from the Li$_2$MnO$_3$ and LiMn$_{0.333}$Ni$_{0.333}$Co$_{0.333}$O$_2$ components, respectively, can be used as a rough guide for determining the Li$_2$MnO$_3$ content in xLi$_2$MnO$_3$·(1 − x)LiMn$_{0.333}$Ni$_{0.333}$Co$_{0.333}$O$_2$ materials, at least for $x \geq 0.1$. A plot of the I_{020}/I_{003} intensity ratio (*C*2/*m*/*R*3$^-$*m*; after background subtraction) as a function of the Li$_2$MnO$_3$ content (wt %) in the xLi$_2$MnO$_3$·(1 − x)LiMn$_{0.333}$Ni$_{0.333}$Co$_{0.333}$O$_2$ series is shown in Figure 3b, in which an enlarged region of the X-ray diffraction pattern of the 0.3Li$_2$MnO$_3$·0.7LiMn$_{0.333}$Ni$_{0.333}$Co$_{0.333}$O$_2$ sample (35 wt % Li$_2$MnO$_3$) is inserted for reference. Corresponding x values and error bars (5%) are also provided in Figure 3b. The plot in Figure 3b is linear, although slightly shifted from the expected ideal plot that would intersect at the origin (0, 0), yielding an excellent goodness of fit (R^2) value of 0.9981.

Acid Treatment. We have previously reported that acid treatment of xLi$_2$MnO$_3$·(1 − x)LiMO$_2$ electrode materials can be used as a method to chemically activate the Li$_2$MnO$_3$ component by leaching Li$_2$O to yield an MnO$_2$ component within the structure, thereby increasing the discharge capacity of the electrode.[24,42] In this study, we therefore focused our investigations on only one acid-treated sample in the series of xLi$_2$MnO$_3$·(1 − x)LiMO$_2$ compounds, namely, $x = 0.3$, to compare the results with and seek differences between this and our earlier related work. We selected this composition, as stated earlier, because if fully activated at high potentials and discharged back to the rock salt stoichiometry, LiMn$_{0.533}$Ni$_{0.233}$Co$_{0.233}$O$_2$, the average manganese oxidation state in the discharged electrode would be 3.44; that is, just marginally below that expected for a potentially damaging Jahn−Teller distortion (3.5).

Acid treatment of 0.3Li$_2$MnO$_3$·0.7LiMn$_{0.333}$Ni$_{0.333}$Co$_{0.333}$O$_2$ with 0.1 M HNO$_3$ for 5 and 24 h removed 17.4 and 20.3% of the lithium, respectively, from the structure (Table 1). The extent of lithium removal is significantly less than that observed when Li$_2$MnO$_3$ is reacted with acid alone,[43,44] indicating that the Li$_2$MnO$_3$ component, when embedded within structurally integrated composite xLi$_2$MnO$_3$·(1 − x)-LiMn$_{0.333}$Ni$_{0.333}$Co$_{0.333}$O$_2$ electrode is more resistant to acid attack. For the 24-h reaction, the pH increased from 1.0 to 3.75, consistent with the removal of lithium from the

(30) Hong, Y.-S.; Park, Y. J.; Wu, X.; Ryu, K. S.; Chang, S. H. *Electrochem. Solid State Lett.* **2003**, *6*, A166.
(31) Yoon, W.-S.; Iannopollo, S.; Grey, C. P.; Carlier, D.; Gorman, J.; Reed, J.; Ceder, G. *Electrochem. Solid State Lett.* **2004**, *7*, A167.
(32) Robertson, A. D.; Bruce, P. G. *Electrochem. Solid State Lett.* **2004**, *7*, A294.
(33) Bregér, J.; Jiang, M.; Dupre, N.; Meng, Y. S.; Shao-Horn, Y.; Ceder, G.; Grey, C. P. *J. Solid State Chem.* **2005**, *178*, 2575.
(34) Chen, Z.; Sun, Y.-K.; Amine, K. *J. Electrochem. Soc.* **2006**, *153*, A1818.
(35) Wu, Y.; Manthiram, A. *Electrochem. Solid State Lett.* **2006**, *9*, A221.
(36) Armstrong, A. R.; Holzapfel, M.; Novak, P.; Johnson, C. S.; Kang, S.-H.; Thackeray, M. M.; Bruce, P. G. *J. Am. Chem. Soc.* **2006**, *128*, 8694.
(37) Shannon, R. D.; Prewitt, C. T. *Acta Crystallogr.* **1969**, *B25*, 925.
(38) Strobel, P.; Lambertandron, B. *J. Solid State Chem.* **1988**, *75*, 90.
(39) Deng, D. L.; Cabaña, J.; Bregér, J. L.; Yoon, W. S.; Grey, C. P. *Chem. Mater.* **2007**, *19*, 6277.
(40) Jeong, S. K.; Song, C.-H.; Nahm, K. S.; Stephan, A. M. *Electrochim. Acta* **2006**, *52*, 885.
(41) Whitfield, P. S.; Davidson, I. J.; Stephens, P. W.; Cranswick, L. M. D.; Swainson, I. P. *Z. Kristallogr. Suppl.* **2007**, *26*, 483.
(42) Kang, S.-H.; Thackeray, M. M. *J. Electrochem. Soc.* **2008**, *155*, A269.
(43) Rossouw, M. H.; Thackeray, M. M. *Mater. Res. Bull.* **1991**, *26*, 463.
(44) Rossouw, M. H.; Liles, D. C.; Thackeray, M. M. *J. Solid State Chem.* **1993**, *104*, 464.

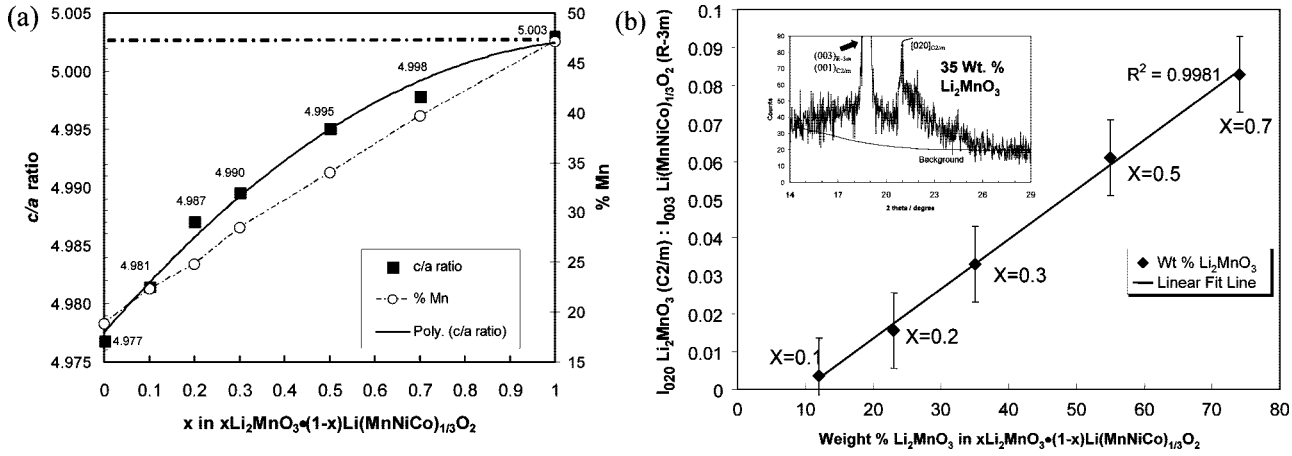

Figure 3. (a) Plot of the *c*/*a* ratio and percent Mn in $x\mathrm{Li_2MnO_3}\cdot(1-x)\mathrm{LiMn_{0.333}Ni_{0.333}Co_{0.333}O_2}$ as a function of composition, x; and (b) plot of the X-ray diffraction intensity ratio of $[020]_{C2/m}$ $\mathrm{Li_2MnO_3}$ component peak to overlapping $[001]_{C2/m} + [003]_{R\bar{3}m}$ peaks of the $\mathrm{Li_2MnO_3}$ and $\mathrm{LiMn_{0.333}Ni_{0.333}Co_{0.333}O_2}$ components as a function of weight percent $\mathrm{Li_2MnO_3}$ in the $x\mathrm{Li_2MnO_3}\cdot(1-x)\mathrm{LiMn_{0.333}Ni_{0.333}Co_{0.333}O_2}$ electrode.

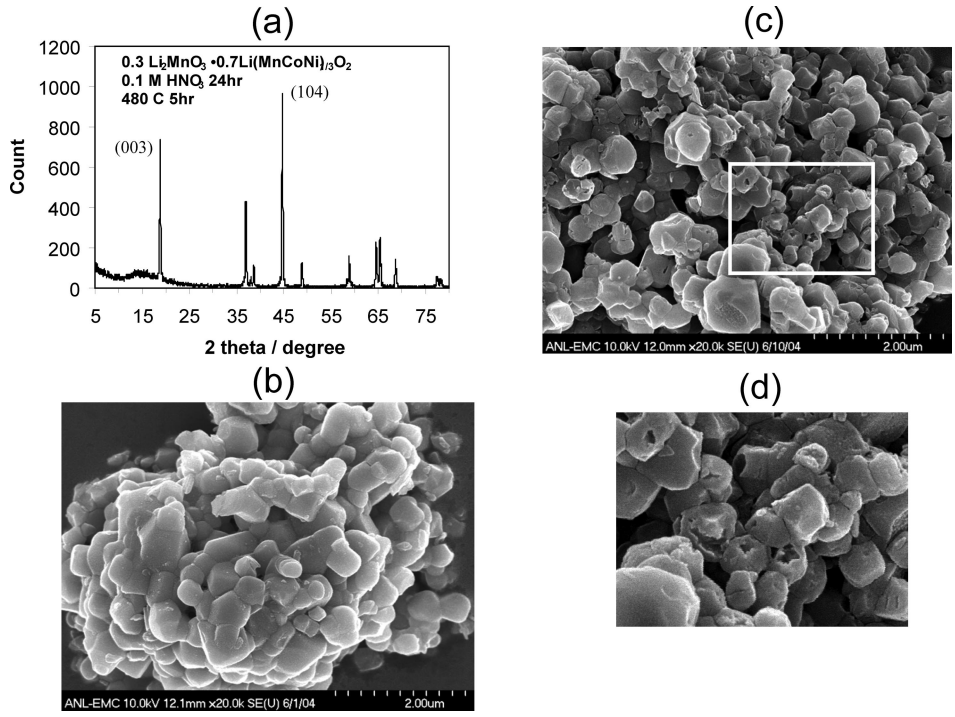

Figure 4. (a) Powder X-ray diffraction pattern of an acid-treated $0.3\mathrm{Li_2MnO_3}\cdot0.7\mathrm{LiMn_{0.333}Ni_{0.333}Co_{0.333}O_2}$ sample after annealing in air at 480 °C; (b, c) scanning electron micrographs of the parent material and its acid-treated product, respectively; and (d) an enlarged view of panel c.

structure into the aqueous solution.[43,45,46] Interestingly, during both 5-h and 24-h reactions, no significant change in the transition metal Mn/Ni/Co ratio was observed, in good agreement with the results of our related study of acid-treated $0.5\mathrm{Li_2MnO_3}\cdot0.5\mathrm{LiMn_{0.31}Ni_{0.44}Co_{0.25}O_2}$ samples.[47] This result implies that redox−dissolution reaction processes do not occur readily in these materials, in contrast to the well-known dissolution of manganese in $\mathrm{LiMn_2O_4}$ that occurs by the disproportionation reaction,

$$2\mathrm{Mn^{3+}} \rightarrow \mathrm{Mn^{4+}} + \mathrm{Mn^{2+}} \quad (1)$$

in which the $\mathrm{Mn^{2+}}$ ions go into solution.[48] The presence of tetravalent manganese and divalent nickel, which tend to be relatively stable in acid,[49,50] is consistent with our result. However, it seems surprising that trivalent cobalt, which tends to be soluble in acid,[51] appears to be insoluble in these composite rock salt structures, at least at room temperature.

The XRD pattern of an acid-treated $0.3\mathrm{Li_2MnO_3}\cdot0.7\mathrm{LiMn_{0.333}Ni_{0.333}Co_{0.333}O_2}$ sample (24-h reaction) and SEM images of the parent and product materials are shown in Figure 4a−d. The diffraction pattern (Figure 4a) shows no evidence of the $\mathrm{H^+}$ ion-exchanged product, $\mathrm{H[Li_{0.333}}$-

(45) Tang, W.; Kanoh, H.; Wang, X.; Ooi, K. *Chem. Mater.* **2000**, *12*, 3271.
(46) Tang, W.; Kanoh, H.; Ooi, K.; Wang, Y. *J. Mater. Chem. Lett.* **2000**, *19*, 1361.
(47) Kang, S.-H.; Johnson, C. S.; Vaughey, J. T.; Amine, K.; Thackeray, M. M. *J. Electrochem. Soc.* **2006**, *153*, A1186.
(48) Hunter, J. C. *J. Solid State Chem.* **1981**, *39*, 142.
(49) Ruetschi, P.; Giovanoli, R. *J. Appl. Electrochem.* **1982**, *12*, 109.
(50) Beverskog, B.; Puigdomenech, I. *Corros. Sci.* **1997**, *39*, 969.
(51) Pourbaix, M. *Atlas d'Equilibres Electrochimiques*; Gauthier-Villars: Paris, 1963.

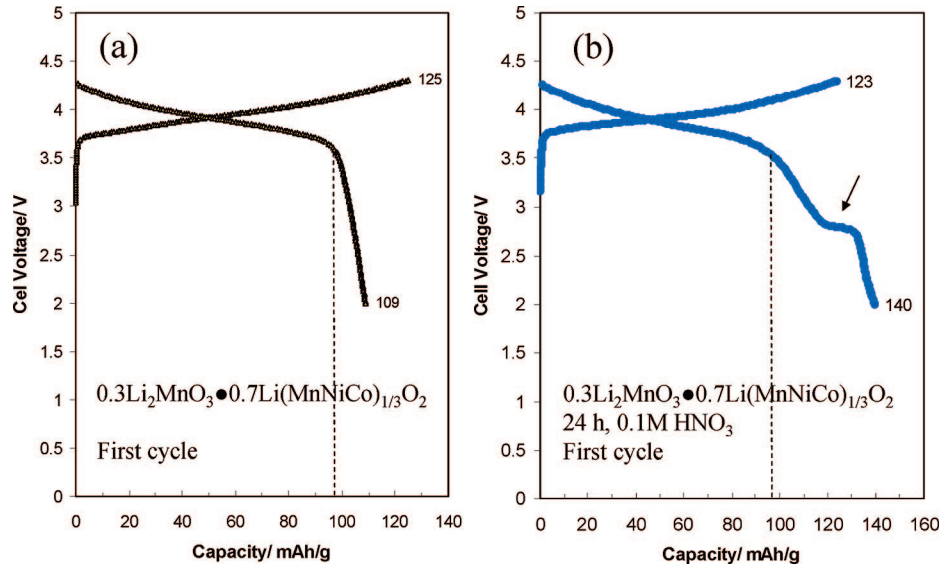

Figure 5. First charge−discharge voltage profiles of lithium half-cells, operated at room temperature between 4.3 and 2.0 V with (a) a parent $0.3Li_2MnO_3 \cdot 0.7$ Li $Mn_{0.333}Ni_{0.333}Co_{0.333}O_2$ electrode and (b) an acid-treated (24 h) electrode. Arrow mark identifies voltage signature arising from the acid-treated Li_2MnO_3 portion of the composite (panel a).

$Mn_{0.333}]O_2$, that is generated during the reaction of bulk Li_2MnO_3 ($Li[Li_{0.333}Mn_{0.333}]O_2$) with acid.[43,52] This result, therefore, provides evidence, at least at this composition ($x = 0.3$) that the Li_2MnO_3-like regions embedded within such composite structures are not readily accessible for H^+ exchange. For higher Li_2MnO_3 concentrations (for example, in $0.7Li_2MnO_3 \cdot 0.3LiMn_{0.5}Ni_{0.5}O_2$ samples), clear evidence of a $H[Li_{0.333}Mn_{0.333}]O_2$ product has been observed.[24]

A comparison of the XRD pattern of the parent $0.3Li_2MnO_3 \cdot 0.7LiMn_{0.333}Ni_{0.333}Co_{0.333}O_2$ compound (Figure 1d) with that of the acid-treated sample (Figure 4a) after annealing at 480 °C to dry the sample reveals that the ratio intensity of the $(003)_{R\bar{3}m}$ peak to the $(104)_{R\bar{3}m}$ reflection is inverted, which reflects the extent to which the layered character of the structure has been disrupted.[53] Note that the XRD patterns of acid-treated products that were dried at 70−100 °C and not subjected to the annealing step did not show this behavior and maintained the dominant $(003)_{R\bar{3}m}$ peak. The XRD pattern in Figure 4a therefore suggests that during the annealing process of the acid-treated samples, some transition metal ions migrate to the lithium layer,[54] which would restrict lithium diffusion and explain our previous observations that acid-treated electrode samples yield high capacities only at a relatively low current rate, typically 0.1 mA/cm^2 or less.[24,47]

Scanning electron microscopy images of the parent $0.3Li_2MnO_3 \cdot 0.7LiMn_{0.333}Ni_{0.333}Co_{0.333}O_2$ compound and acid-treated product are shown in Figure 4b and c, respectively. Whereas the parent material is composed of well-rounded and agglomerated (sintered) particles, the acid-treated sample shows clear evidence of corrosion and distinct pitted regions, clearly visible in the enlarged SEM image (Figure 4d) that can be attributed largely to the dissolution of lithium from the particles. Note, however, that if there had been dissolution of transition metal ions during acid treatment, then the AES-ICP data in Table 1 indicate that Mn, Ni, and Co ions would have dissolved in the same ratio present in the original structure, which seems an unlikely possibility.

Electrochemical Characterization. Electrochemical evaluations of $xLi_2MnO_3 \cdot (1 - x)LiMn_{0.333}Ni_{0.333}Co_{0.333}O_2$ electrodes were performed in lithium half-cells. The cells were charged and discharged at 0.1 mA/cm^2, between either 4.3 and 2.0 V or 4.6 and 2.0 V, to monitor the differences in the electrochemical behavior of unactivated electrodes against electrochemically activated and chemically activated (acid-treated) electrodes. For 4.6−2.0 V cycling, tests were conducted both at room temperature and at 50 °C, because the higher temperature operation aided the rate of the reaction and the extent to which the Li_2MnO_3 component could be delithiated (activated).[25]

4.3−2.0 V Cycling at Room Temperature. When cells were cycled between 4.3 and 2.0 V, the capacity of the $xLi_2MnO_3 \cdot (1 - x)LiMn_{0.333}Ni_{0.333}Co_{0.333}O_2$ electrodes decreased with increasing x, that is, with increasing Li_2MnO_3 content. This result was expected because the Li_2MnO_3 component is electrochemically inactive within this voltage range. The voltage profile of a typical $Li/xLi_2MnO_3 \cdot (1 - x)LiMn_{0.333}Ni_{0.333}Co_{0.333}O_2$ cell operated at room temperature is shown for $x = 0.3$ in Figure 5a, together with a corresponding acid treated sample (Figure 5b). In Figure 6, the drop in electrode capacity for untreated $Li/xLi_2MnO_3 \cdot (1 - x)LiMn_{0.333}Ni_{0.333}Co_{0.333}O_2$ cells ($0 \le x \le 0.3$) as a function of x is shown in capacity vs cycle number plots of the various cells. Note that although the capacity decreases with increasing Li_2MnO_3 content, the cells cycle with greater stability, consistent with the premise that the Li_2MnO_3 component serves to stabilize layered $LiMO_2$ electrode structures.[1,3,23,55] For example, the $LiMn_{0.333}Ni_{0.333}Co_{0.333}O_2$ ($x = 0$) electrode, which delivered 154 mAh/g after 18 cycles, showed a fade rate of 0.78% mAh/g/cycle between cycles 2 and 18, whereas

(52) Paik, Y.; Grey, C. P.; Johnson, C. S.; Kim, J.-S.; Thackeray, M. M. *Chem. Mater.* **2002**, *14*, 5109.
(53) Tran, N.; Croguennec, L.; Labrugere, C.; Jordy, C.; Biensan, Ph.; Delmas, C. *J. Electrochem. Soc.* **2006**, *153*, A261.
(54) Morales, J.; Peres-Vicente, C.; Tirado, J. L. *Mater. Res. Bull.* **1990**, *25*, 623.

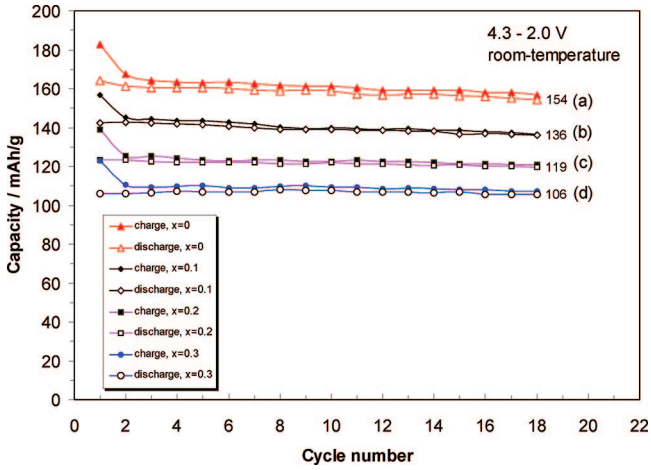

Figure 6. Specific capacity vs cycle number plots for xLi$_2$MnO$_3$·$(1-x)$-LiMn$_{0.333}$Ni$_{0.333}$Co$_{0.333}$O$_2$ electrodes, obtained at room temperature between 4.3 and 2.0 V for (a) $x = 0$, (b) $x = 0.1$, (c) $x = 0.2$, and (d) $x = 0.3$.

the 0.3Li$_2$MnO$_3$·0.7LiMn$_{0.333}$Ni$_{0.333}$Co$_{0.333}$O$_2$ ($x = 0.3$) electrode delivered a constant 106 mAh/g over its first 18 cycles.

The voltage profiles of the initial charge/discharge cycle between 4.3 and 2.0 V of Li/0.3Li$_2$MnO$_3$·0.7LiMn$_{0.333}$Ni$_{0.333}$Co$_{0.333}$O$_2$cells with untreated and acid-treated electrodes are distinctly different (Figure 5a and b). Although the initial charge capacity was essentially the same for the two cells (125 and 123 mAh/g, respectively) and although both electrodes delivered approximately ~95−100 mAh/g when discharged to 3.5 V, the acid-treated electrode provided a significantly higher capacity (140 mAh/g) when discharged to 2.0 V, as compared to the unactivated parent electrode (109 mAh/g). This difference in behavior is a result of the chemical activation process whereby Li$_2$O is removed from the Li$_2$MnO$_3$ component of the composite electrode structure to yield an electrochemically active MnO$_2$ component.[27,36,56−58] The additional capacity delivered by the activated electrode and the shape of the voltage profile between 3.5 and 2.0 V will be addressed in more detail in the discussion on the 4.6−2.0 V cycling of these cells that follows below.

4.6−2.0 V Cycling at Room Temperature. Typical voltage profiles of the initial and 15th cycles of Li/0.3Li$_2$MnO$_3$·0.7LiMn$_{0.333}$Ni$_{0.333}$Co$_{0.333}$O$_2$ cells with untreated and acid-treated electrodes, charged and discharged between 4.6 and 2.0 V in lithium half-cells at room temperature, are shown as examples in Figure 7a and b, respectively. It is immediately clear from the figures that raising the charging potential to 4.6 V results in significantly higher charge and discharge capacities from both electrochemically activated and chemically activated electrodes compared to electrodes cycled between 4.3 - 2.0 V (Figure 5a and b). The electrochemically activated electrodes yield a significantly superior cycling stability but inferior first-cycle efficiency relative to the acid-treated electrodes, consistent with our earlier reports.[24,47,55] The large first-cycle capacity loss observed in cells with untreated electrodes has been attributed to the electrochemical removal of two lithium ions per Li$_2$MnO$_3$ unit above 4.3 V during charge and to the reinsertion of only one lithium ion into the resulting MnO$_2$ component during discharge.[23,36] Chemical activation, on the other hand, leaches Li$_2$O from the Li$_2$MnO$_3$ component prior to cell assembly, thereby resulting in an improved coulombic efficiency of the cell in the first cycle. The relatively poor cycling stability of the acid-treated electrode is attributed to the migration of transition metal cations into the lithium layer during the annealing (drying) step of the electrode, as described earlier, and to possible surface damage.[42] Of particular significance to this study is that the capacity delivered by the acid-treated electrodes on the plateau below 3 V (~40 mAh/g) on the initial discharge is essentially independent of the upper voltage charging limit (4.3 or 4.6 V), thereby confirming the extent of Li$_2$O removal during chemical activation (arrow marks in Figures 5b and 7b).

Capacity vs cycle number plots of xLi$_2$MnO$_3$·$(1-x)$-LiMn$_{0.333}$Ni$_{0.333}$Co$_{0.333}$O$_2$ electrodes for $x = 0$, 0.1, 0.2, and 0.3 when cycled between 4.6 and 2.0 V are compared in Figure 8. The data demonstrate that a significant performance improvement, not only in cycling stability but also in capacity, is provided by electrodes containing a higher Li$_2$MnO$_3$ content, notably xLi$_2$MnO$_3$·$(1-x)$LiMn$_{0.333}$Ni$_{0.333}$Co$_{0.333}$O$_2$ electrodes ($x = 0.3$). The data therefore give further credence to our premise that increasing the Mn content within integrated xLi$_2$MnO$_3$·$(1-x)$LiMO$_2$ structures provides a strategy for increasing the capacity and stability of layered LiMO$_2$ electrodes, particularly at high potentials.[1,3]

Cyclic Voltammetry. Cyclic voltammograms of xLi$_2$MnO$_3$·$(1-x)$LiMn$_{0.333}$Ni$_{0.333}$Co$_{0.333}$O$_2$ electrodes were recorded at a sweep rate of 0.02 mV/s between 5.0 and 2.0 V for $x = 0$ and 0.3 and its acid-treated product (Figure 9a−c) in an attempt to gather information about the individual redox process that occurs during charge and discharge. The overall features of the CVs for $x = 0$ and 0.3 are, in general, the same. The similarity in the current/potential profiles is attributed to the AES-ICP compositional analyses that had shown that the excess lithium used to counter evaporative losses had remained in the samples, making the standard sample ($x = 0$), in particular, slightly lithium-rich (Table 1). In these CVs, the first anodic peak at approximately 4.0 V on the initial cycle is associated predominantly with Ni oxidation from Ni^{2+} to Ni^{4+}, and the second peak at higher potential (~4.6−4.7 V) is associated predominantly with the irreversible electrochemical activation reaction that strips Li$_2$O from the Li$_2$MnO$_3$ component to form MnO$_2$.[24,31,36,47,59] At least partial oxidation of Co^{3+} to Co^{4+} could also occur during these two processes. Two cathodic peaks are evident on discharge. Although it is impossible to differentiate the reduction processes (* marks in Figure 9a, b, and c) of the individual Mn, Ni, and Co ions from this data, it is believed from theoretical and NMR studies that the process at ~4.5 V may be associated with the occupation of tetrahedral sites by lithium within the extensively delithiated (lithium) layer and the lower voltage processes between 3.0 and 3.6 V to

(55) Kim, J.-S.; Johnson, C. S.; Thackeray, M. M. *Electrochem. Commun.* **2002**, *4*, 205.
(56) Johnson, C. S.; Thackeray, M. M. *Interfaces, Phenomena, and Nanostructures in Lithium Batteries*, ed.; Landgrebe, A., Klingler, R. J., Eds.; The Electrochemical Society Inc.: Pennington, NJ, Proceedings Volume 2001, *2000−36*, 47.
(57) Johnson, C. S. *J. Power Sources* **2007**, *165*, 559.
(58) Kang, S.-H.; Kempgens, P.; Greenbaum, S.; Kropf, A. J.; Amine, K.; Thackeray, M. M. *J. Mater. Chem.* **2007**, *17*, 2069.
(59) Lu, Z.; Dahn, J. R. *J. Electrochem. Soc.* **2002**, *149*, A815.

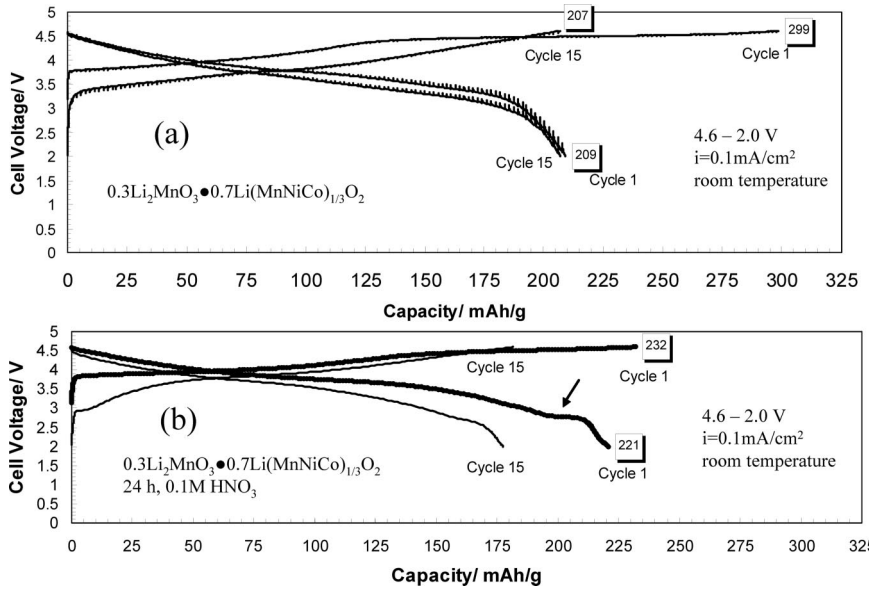

Figure 7. Electrochemical cycling profiles of the initial and 15th cycles of lithium half-cells, operated at room temperature between 4.6 and 2.0 V, containing (a) a parent $0.3Li_2MnO_3 \cdot 0.7LiMn_{0.333}Ni_{0.333}Co_{0.333}O_2$ electrode and (b) an acid-treated (24 h) electrode. Arrow mark identifies voltage signature arising from the acid-treated Li_2MnO_3 portion of the composite (Figure 7b).

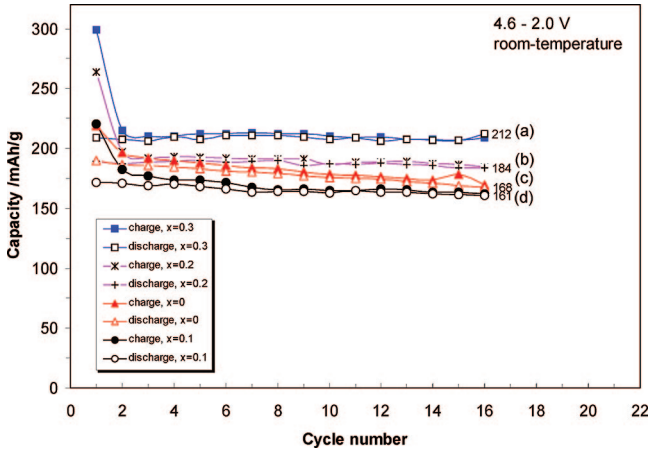

Figure 8. Specific capacity vs cycle number plots for $xLi_2MnO_3 \cdot (1-x)LiMn_{0.333}Ni_{0.333}Co_{0.333}O_2$ electrodes obtained at room temperature between 4.6 and 2.0 V for (a) $x = 0.3$, (b) $x = 0.2$, (c) $x = 0$, and (d) $x = 0.1$.

the occupation of octahedral sites, in agreement with the reports of Hayley et al.[60] and Bregér et al.[61] It is evident that both reaction processes are reversible. By contrast, the CV of the acid-treated electrode ($x = 0.3$) in Figure 9c shows a third reversible redox peak (marked with a circumflex in Figure 9c) below 3 V, consistent with the lithiation/delithiation of a chemically derived MnO_2 component in the electrode, which is distinct from the MnO_2 component derived electrochemically. These data are in good agreement with the results of Kang et al. in their study of fluorinated $0.5Li_2MnO_3 \cdot 0.5LiMn_{0.31}Ni_{0.44}Co_{0.25}O_2$ electrodes.[26] Little information is known at this stage about the structural character of the MnO_2 components formed electrochemically and chemically, but it is clear from recent high-resolution transmission electron microscopy studies that these materials, both as-prepared and electrochemically cycled, are extremely complicated.[62,63] However, the profiles of the cyclic voltammograms in Figure 9a−c suggest that when electrochemically activated, the MnO_2 component retains the layered character of the parent structure, at least during the early cycles of the cell, whereas when chemically activated, the MnO_2 regions have both layered and apparent spinel-like character. Thus, we conclude that the MnO_2-rich component created by lithia removal during the electrochemical reaction is structurally different from that produced by chemical treatment with acid. Note that the higher the manganese content in $xLi_2MnO_3 \cdot (1-x)LiMn_{0.333}Ni_{0.333}Co_{0.333}O_2$ electrodes (i.e., the higher the value of x), the more probable it is that layered to spinel transformations will occur in localized regions of the structure. Such transformations will be irreversible, but may aid to stabilize these complex layered electrodes to further lithium insertion/extraction reactions.

4.6−2.0 V Cycling at 50 °C. Electrochemical experiments of $Li/xLi_2MnO_3 \cdot (1-x)LiMn_{0.333}Ni_{0.333}Co_{0.333}O_2$ cells were also conducted at 50 °C to aid the kinetics of the electrochemical reaction, particularly within the $xLi_2MnO_3 \cdot (1-x)LiMn_{0.333}Ni_{0.333}Co_{0.333}O_2$ electrodes.[25] For these tests, cells were charged and discharged between 4.6 and 2.5 V at 0.1 mA/cm^2 to monitor the initial activation and subsequent process and between 4.6 and 2.0 V to determine their cycling stability. Voltage profiles of the initial charge/discharge cycle of cells are plotted for $x = 0$, 0.1, 0.3, 0.5, and 0.7 in Figure 10. The extent of the initial charge reaction between 3.0 and 4.4 V, which is associated with lithium extraction from the $LiMn_{0.333}Ni_{0.333}Co_{0.333}O_2$ component, decreases with increasing x, whereas the voltage plateau at ~4.4−4.6 V, which is attributed to the activation of the Li_2MnO_3 component, lengthens with increasing x, as expected. Although polariza-

(60) Hayley, H. H.; Yabuuchi, N.; Meng, Y. S.; Kumar, S.; Bregér, J.; Grey, C. P.; Shao-Horn, Y. *Chem. Mater.* **2007**, *19*, 2551.
(61) Bregér, J.; Meng, Y. S.; Hinuma, Y.; Kumar, S.; Kang, K.; Shao-Horn, Y.; Ceder, G.; Grey, C. P. *Chem. Mater.* **2006**, *18*, 4768.
(62) Weill, F.; Tran, N.; Martin, N.; Croguennec, L.; Delmas, C. *Electrochem. Solid State Lett.* **2007**, *10*, A194.
(63) Lei, C. H.; Bareno, J.; Wen, J. G.; Petrov, I.; Kang, S. H.; Abraham, D. P. J. *Power Sources* **2008**, *178*, 422.

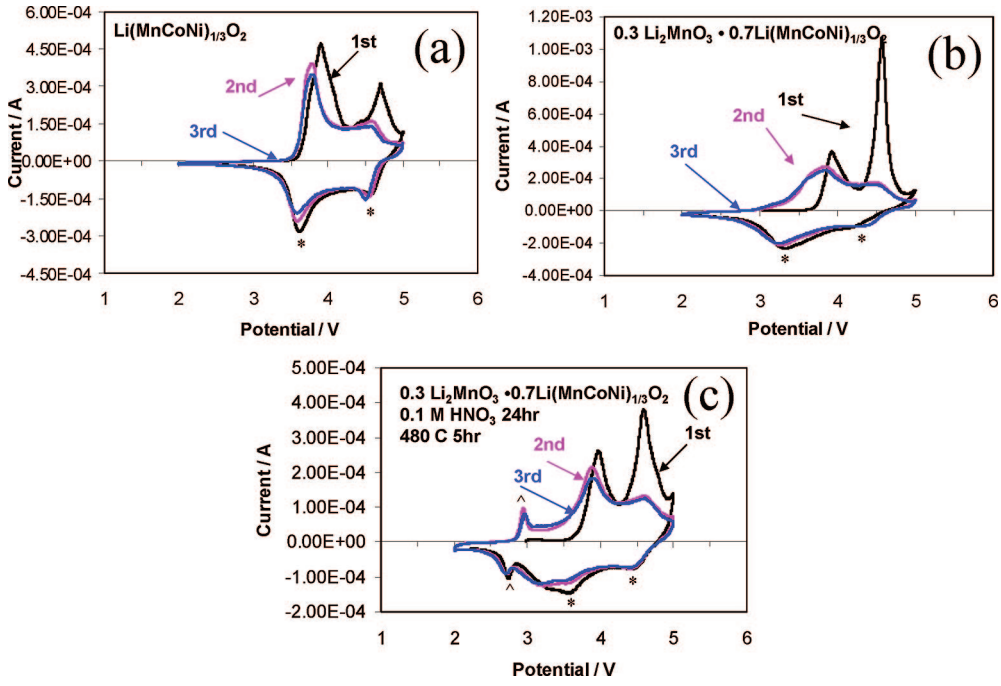

Figure 9. Cyclic voltammograms of $xLi_2MnO_3 \cdot (1 - x)LiMn_{0.333}Ni_{0.333}Co_{0.333}O_2$ electrodes for (a) $x = 0$, (b) $x = 0.3$, and (c) $x = 0.3$, acid-treated (24 h).

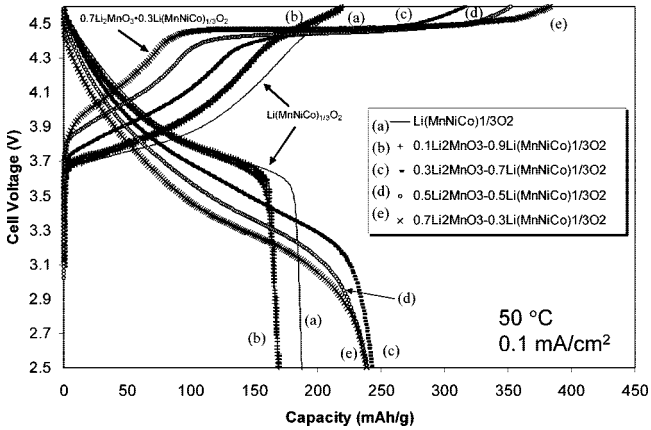

Figure 10. Initial charge−discharge voltage profiles of $Li/xLi_2MnO_3 \cdot (1 - x)LiMn_{0.333}Ni_{0.333}Co_{0.333}O_2$ half-cells operated at 50 °C between 4.6 and 2.5 V at 0.1 mA/cm^2 for (a) $x = 0$, (b) $x = 0.1$, (c) $x = 0.3$, (d) $x = 0.5$, and (e) $x = 0.7$.

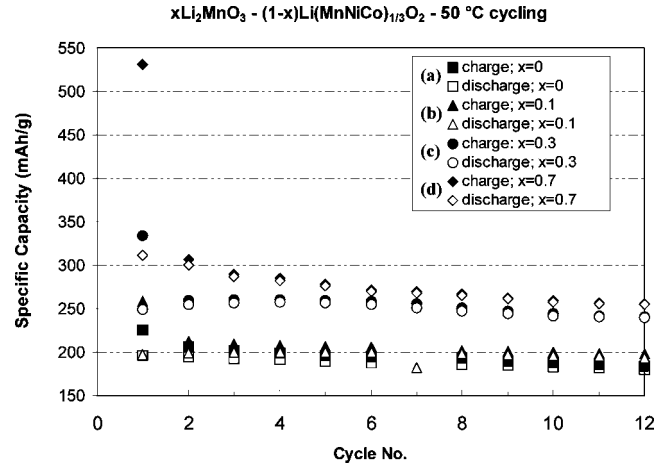

Figure 11. Specific capacity vs cycle number plots for $xLi_2MnO_3 \cdot (1 - x)LiMn_{0.333}Ni_{0.333}Co_{0.333}O_2$ electrodes, obtained at 50 °C between 4.6 and 2.0 V at 0.0.05 mA/cm^2 for (a) $x = 0$, (b) $x = 0.1$, (c) $x = 0.3$, and (d) $x = 0.7$.

tion is most severe for electrodes with the highest Mn content ($x = 0.3$, 0.5, and 0.7) on both charge and discharge, they deliver a significantly higher discharge capacity (~250 mAh/g) than electrodes with lower Mn content ($x = 0$ and 0.1), which deliver less than 200 mAh/g.

By lowering the current rate to 0.05 mA/cm^2, even higher charge/discharge capacities can be achieved. Anomalously high-capacity values above the theoretically expected values can be obtained from $xLi_2MnO_3 \cdot (1 - x)LiMn_{0.333}Ni_{0.333}Co_{0.333}O_2$ electrodes with a high manganese content (~250 mAh/g), typically those in which $0.5 \leq x \leq 0.7$, particularly during the early charge/discharge cycles.[25] Although the origin of these exceptionally high capacities is not yet known, it has been speculated that the anomalous capacity is due in part to products of electrolyte oxidation reactions at high potentials; possible trapping of oxygen gas, released during the electrochemical activation process, within the activated electrode particles;[25,64] or oxidation of manganese ions above the tetravalent state.[65] Capacity vs cycle number plots for $Li/xLi_2MnO_3 \cdot (1 - x)LiMn_{0.333}Ni_{0.333}Co_{0.333}O_2$ cells ($x = 0$, 0.1, 0.3, and 0.7) that had been charged and discharged at 0.05 mA/cm^2 are provided in Figure 11. The data again emphasize that Li_2MnO_3-stabilized $LiMn_{0.333}Ni_{0.333}Co_{0.333}O_2$ electrodes can provide exceptionally high capacities for the higher values of x. Note that for both $x = 0.3$ and 0.7, the cells deliver a reasonably steady capacity of ~250 mAh/g at 0.05 mA/cm^2, which closely approximates the theoretically expected values of the two electrodes based on the mass of

(64) Ogasawara, T.; Debert, A.; Holzapfel, M.; Novak, P.; Bruce, P. G. *J. Am. Chem. Soc.* **2006**, *128*, 1390.
(65) Kalyani, P.; Mitra, S.; Mohan, T.; Gopukumar, S. *J. Power Sources* **1999**, *80*, 103.

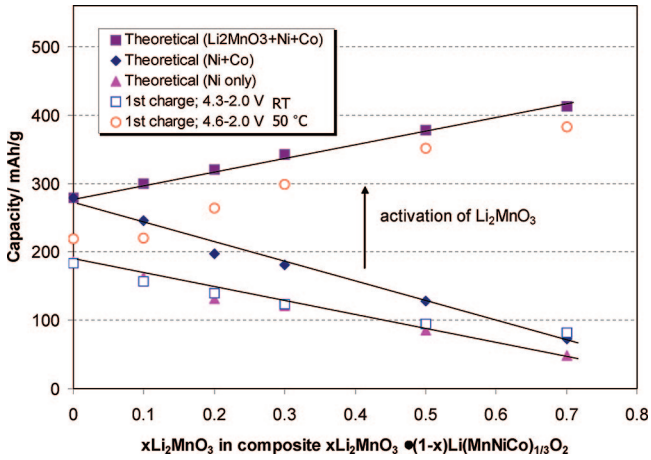

Figure 12. Theoretical and experimental charge capacities delivered by $x\mathrm{Li_2MnO_3}\cdot(1-x)\mathrm{LiMn_{0.333}Ni_{0.333}Co_{0.333}O_2}$ electrodes as a function of the cell cutoff voltage (4.3 or 4.6 V vs $\mathrm{Li^0}$) and electrode composition, x.

the starting electrodes (namely, 262 and 243 mAh/g, respectively) if completely delithiated during electrochemical activation.

Pure $\mathrm{Li_2MnO_3}$ electrodes can be activated above 4.4 V, but they cycle with relatively poor efficiency and lose capacity steadily.[66] The high reversible capacity delivered by the $0.7\mathrm{Li_2MnO_3}\cdot0.3\mathrm{LiMn_{0.333}Ni_{0.333}Co_{0.333}O_2}$ electrode shown in Figure 11 is, therefore, particularly noteworthy because it illustrates that a relatively small amount of a $\mathrm{LiMn_{0.333}Ni_{0.333}Co_{0.333}O_2}$, is sufficient to stabilize a $\mathrm{Li_2MnO_3}$ electrode to electrochemical cycling when charged to high potentials.

Figure 12 shows a plot of the theoretical capacities of $x\mathrm{Li_2MnO_3}\cdot(1-x)\mathrm{LiMn_{0.333}Ni_{0.333}Co_{0.333}O_2}$ electrodes when electrochemically activated and completely delithiated during an initial charge; the figure also shows the experimentally determined values when the electrodes were initially charged to 4.3 V at room temperature and when charged to 4.6 V at 50 °C. Theoretical capacities were calculated assuming the following oxidation/activation reactions: (i) $\mathrm{Ni^{2+}} \rightarrow \mathrm{Ni^{4+}}$ (black triangles), (ii) $\mathrm{Ni^{2+}} \rightarrow \mathrm{Ni^{4+}}$ and $\mathrm{Co^{3+}} \rightarrow \mathrm{Co^{4+}}$ (black diamonds), and (ii) $\mathrm{Ni^{2+}} \rightarrow \mathrm{Ni^{4+}}$; $\mathrm{Co^{3+}} \rightarrow \mathrm{Co^{4+}}$ and $\mathrm{Li_2MnO_3}$ activation/$\mathrm{Li_2O}$ loss (black squares). The experimental capacities determined for the various values of x are shown as open squares for cells charged to 4.3 V, and open circles when charged to 4.6 V. For cells charged to 4.3 V, the data indicate that the initial reaction closely tracks nickel oxidation alone, at least to $x = 0.3$, and thereafter, for higher manganese content, cobalt becomes more prominent in participating in the reaction. When charged to 4.6 V at 50 °C, the experimentally determined capacities fall short of the theoretical values; this result is attributed to the difficulty in electrochemically activating all of the $\mathrm{Li_2MnO_3}$ component without interference from other extraneous capacity generation effects or side-reactions at 4.4−4.6 V, such as electrolyte oxidation.

Finally, it is worthwhile to comment on the evolving charge/discharge profile of a $\mathrm{Li}/0.7\mathrm{Li_2MnO_3}\cdot0.3\mathrm{LiMn_{0.333}Ni_{0.333}Co_{0.333}O_2}$ cell that was cycled between 4.6 and 2.0 V

(66) Johnson, C. S.; Li, N.; Vaughey, J. T.; Thackeray, M. M. *Electrochem. Commun.* **2005**, *7*, 528.

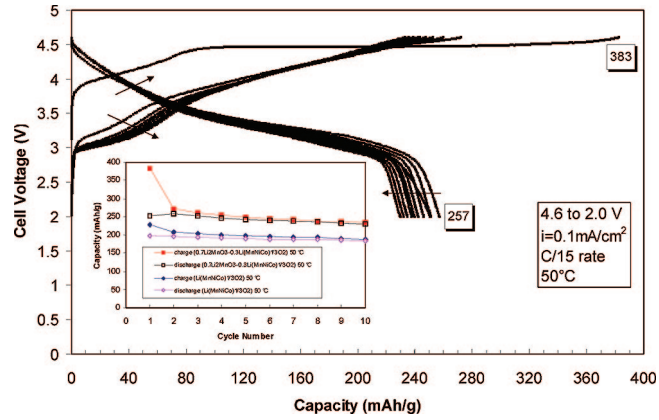

Figure 13. Evolving spinel-like voltage profile during charge in a lithium half-cell with a high manganese content $0.7\mathrm{Li_2MnO_3}\cdot0.3\mathrm{LiMn_{0.333}Ni_{0.333}Co_{0.333}O_2}$ electrode. Inset provides the capacity cycling data with cycle number for $x = 0.7$ and $x = 0$ Li cells.

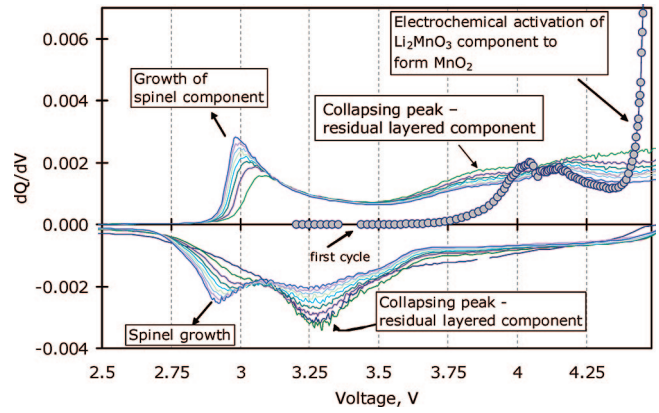

Figure 14. dQ/dV derivative plot of the voltage profile shown in Figure 13 for a $\mathrm{Li}/0.7\mathrm{Li_2MnO_3}\cdot0.3\mathrm{LiMn_{0.333}Ni_{0.333}Co_{0.333}O_2}$ cell.

at 50 °C at 0.1mA/cm^2 (Figure 13). First, the capacity versus cycle number from 1 to 10 is plotted in the inset to the figure. The capacity for $x = 0.7$ is 25% higher (230 mAh/g) than the standard $x = 0$ material (184 mAh/g), indicating a significant capacity contribution from the electrochemically activated $\mathrm{Li_2MnO_3}$-like portion of the composite. Second, the sloping discharge profile between 4.5 and 3 V is, at first sight, suggestive of single-phase behavior, whereas the charge profile shows increasing two-phase behavior. The two-phase behavior on discharge is more apparent in the dQ/dV plots of the cell (Figure 14), in which the evolution of a dominant reversible redox reaction slightly below 3 V after the initial electrochemical activation of the $\mathrm{Li_2MnO_3}$ component above 4.4 V occurs at the expense of the redox reaction of the parent layered structure (3.3 V/3.9 V), suggesting that the layered $0.7\mathrm{Li_2MnO_3}\cdot0.3\mathrm{LiMn_{0.333}Ni_{0.333}Co_{0.333}O_2}$ electrode transforms in regions to spinel on cycling to yield a layered-spinel intergrowth structure.[66] Of particular interest is the apparent absence of a strong redox peak at 4.1 V that would correspond to the removal of lithium from the tetrahedral sites of an evolving spinel-like component. This discrepancy is attributed tentatively to the complex cation arrangement within the intergrown layered-spinel structure that allows the lithium insertion/extraction reactions to be associated predominantly with the filling/emptying of octahedral sites rather than tetrahedral sites. A layered-to-spinel

transformation, however, is not unexpected for electrodes with such a high manganese content because layered $LiMnO_2$ and its substituted derivatives are known to transform electrochemically to spinel in lithium cells.[67,68]

Conclusions

Structurally integrated electrodes, represented by the general formula $xLi_2MnO_3 \cdot (1-x)LiMn_{0.333}Ni_{0.333}Co_{0.333}O_2$, have been investigated in lithium half-cells over two voltage ranges; namely, 4.3−2.0 and 4.6−2.0 V, for a wide compositional range ($0 \leq x \leq 0.7$). Capacity vs cycle number plots confirm unequivocally that the Li_2MnO_3 component serves to stabilize $LiMn_{0.333}Ni_{0.333}Co_{0.333}O_2$ electrodes to electrochemical cycling. If the Li_2MnO_3 component is activated above 4.4 V, then extremely high initial discharge capacities (~250 mAh/g) can be achieved relative to standard $LiMn_{0.333}Ni_{0.333}Co_{0.333}O_2$ electrodes (~180−190 mAh/g), but only at relatively low rates. $xLi_2MnO_3 \cdot (1-x)LiMn_{0.333}Ni_{0.333}Co_{0.333}O_2$ electrodes, particularly those with a high manganese content, appear to transform to spinel, at least in localized regions of the electrode, without significantly affecting cycling stability. The study also demonstrates that at $x = 0.7$, a relatively low concentration of $LiMn_{0.333}Ni_{0.333}Co_{0.333}O_2$ is adequate for stabilizing, in turn, a Li_2MnO_3 electrode that has been charged to high potentials (>4.4 V). This finding has implications for stabilizing other metal oxide electrodes normally believed to be unstable to lithium insertion/extraction reactions.

Acknowledgment. Financial support from the Office of Vehicle Technologies of the U.S. Department of Energy under Contract DE-AC02-06CH11357 is gratefully acknowledged.

The submitted manuscript has been created by UChicago Argonne, LLC, Operator of Argonne National Laboratory ("Argonne"). Argonne, a U.S. Department of Energy Office of Science laboratory, is operated under Contract No. DE-AC02-06CH11357.

CM801245R

(67) Shao-Horn, Y.; Hackney, S. A.; Armstrong, A. R.; Bruce, P. G.; Gitzendanner, R.; Johnson, C. S.; Thackeray, M. M. *J. Electrochem. Soc.* **1999**, *146*, 2404.

(68) Armstrong, A. R.; Paterson, A. J.; Dupré, N.; Grey, C. P.; Bruce, P. G. *Chem. Mater.* **2007**, *19*, 1016.